ORIGINAL ARTICLE

On-Orbit Observations of Conjuncting Space Objects Prior to the Time of Closest Approach

Robert Lauchie Scott[1] · Stefan Thorsteinson[1] · Viqar Abbasi[2]

Abstract

Conjunction assessment of space objects in Low Earth Orbit (LEO) generally uses information collected by ground-based space surveillance sensors. These sensors track both the *primary* object (normally an active satellite) and the *secondary* object (typically space debris). The tracking data is used to update both objects' orbits for collision risk assessment. The primary satellite's involvement in this process is that of a satellite in jeopardy - the primary satellite does not usually contribute tracking data on the secondary as they are typically unequipped to do so. In this paper, an examination how an at-risk LEO primary satellite could obtain optical tracking data on a secondary object prior to the Time of Closest Approach (TCA) and assess its own collision risk without the need for additional ground-based space surveillance data is performed. This analysis was made possible by using in-situ optical measurements of space objects conjuncting with the Canadian NEOSSat Space Situational Awareness R&D microsatellite. By taking advantage of the near "constant-bearing, decreasing range" observing geometry formed during a LEO conjunction, NEOSSat can collect astrometric and photometric measurements of the secondary object in the time prior to TCA, or in the multiple half-orbits preceding TCA. This paper begins by describing the in-situ phenomenology of optically observed conjunctions in terms of the observing approach, geometry and detected astrometric and photometric characteristics. It was found that conjuncting objects are detectable to magnitude 16 and astrometric observations can be used for position covariances in the computation of probability of collision. Illustrative examples are provided. In orbits prior to TCA, in-track positioning error is improved by a factor of two or more by processing space-based

✉ Robert Lauchie Scott
   Lauchie.Scott@drdc–rddc.gc.ca

1   Defence R&D Canada Ottawa, 3701 Carling Avenue, Ottawa, ON K1A 0Z4, Canada

2   Canadian Space Agency, 6767 Route d'Aeroport, St. Hubert, QC J3Y 8Y9, Canada

observations on a filtered position estimate of the secondary. However, cross-track positioning knowledge is negligibly improved due to the inherent astrometric measurement precision of the NEOSSat sensor and the oblique observing geometry during conjunction observations. A short analysis of object detectability where star trackers could be used to perform similar observations finds that larger payload-sized objects would generally be detectable. However, smaller debris objects would require higher sensitivity from the star tracker if employed for optical conjunction derisk observations.

Introduction

Satellite operators are continuing to manage the increasing number of conjunction (close approach) warnings due to the growing number of debris objects in Earth orbit. In Canada, operators of space assets in Low Earth Orbit (LEO) rely on conjunction warnings provided by the US Air Force's 18th Space Control Squadron (18th SPCS) which use orbital data collected by the Space Surveillance Network (SSN) [1]. The 18th SPCS offers Advanced Screening services [1, 2], providing conjunction warnings forecasted up to 7 days in advance of the Time of Closest Approach (TCA) providing operators increased time to analyze collision risk and create manuever plans. These warnings take the form of Conjunction Data Messages (CDMs), a standardized text format enabling rapid evaluation of collision risk of two space objects [1]. In the lead-up to TCA, space surveillance sensors acquire increased tracking data on both space objects increasing their positioning knowledge and help validate the actual risk. Risk is generally estimated by computing the Probability of Collision (PoC) that two space objects could collide based on the primary and secondary's orbital position covariance and their spherical hard-body radii. In Canadian space operations a PoC exceeding 10^{-6} is considered to be a "warning" criteria prompting increased monitoring of the two objects' conjunction. PoCs exceeding 10^{-4} are considered "action" criteria by both the Canadian Space Operations Centre (CanSpOC) and the Canadian Space Agency's Satellite Operations team. PoCs exceeding 10^{-4} triggers enhanced orbital analysis or debris avoidance maneuvers [2, 3] if the satellite has the capability to manuever.

This model of conjunction assessment works relatively well for the current population of space objects. However, this technique inherently relies on tracking data collected by ground-based sensors in the time prior to TCA. The primary satellite does not contribute to the risk assessment, nor does it collect observations on the secondary during the days (or hours) leading up to the conjunction. The conjunction event itself is generally unobserved by Space Situational Awareness (SSA) sensors to validate that the objects safely passed one another. The collision avoidance process is also hindered by infrequent ground station accesses limiting the number of opportunities that a satellite operator can upload maneuver commands in response to new orbital data. In an era of upcoming mega-constellations, satellite operators may not be able to provide the individual attention required for each constellation asset for conjunction assessment. This will likely force the use of automation and independent tracking data as a requirement for future space systems to help mitigate orbital collision risk. In this paper, an expanded question is asked: *Can a satellite take optical observations on conjuncting space objects to independently assess the risk of collision?*

In 2018, NEOSSat, a Space Situational Awareness (SSA) microsatellite, jointly operated by the Canadian Space Agency and Defence R&D Canada, began a series of observational experiments observing space objects conjuncting with it. The intent of this experimentation was to optically characterize conjuncting space objects to determine if self-protection is a possibility if enough onboard computational autonomy were available to track, detect and estimate orbits. While NEOSSat does not have the on-board computational capabilities to independently update a conjuncting space object's orbit nor does it have a propulsion system to perform debris avoidance maneuvers if a collision risk threatens - an analysis of rapid encounter observing strategies is of value. This paper begins by describing the in-situ phenomenology of optically observed conjunctions in terms of their approach geometry, observing techniques, and the detected astrometric and photometric properties of the secondary. We then examine how a LEO satellite, equipped with an optical space surveillance sensor, could contribute to the collision avoidance process, rather than being a passive satellite-at-risk. It was found that observing opportunities on the secondary object regularly occur in the *half-orbit* intersections prior to conjunction. An examination of how this half-orbit technique can be used in real-life conjunction scenarios is explored, limitations described and how possible adaptation of star trackers could be employed to perform conjunction derisk observations from a detectability perspective.

Characteristics of NEOSSAT Conjunctions

NEOSSat is a 74 kg space telescope of overall dimensions of $1.37 \times 0.78 \times 0.38$ m [4]. NEOSSat's 785 km altitude orbit borders the densest part of the LEO orbital debris environment leading to regular conjunctions with a variety of payload and debris objects. The frequency of space object conjunction events with NEOSSat varies, but the historical average is ~1 conjunction event/week based on the 1x1x1 km³ screening volume used by the 18th SPCS. Figure 1 shows the top 40 objects frequently conjuncting with NEOSSat
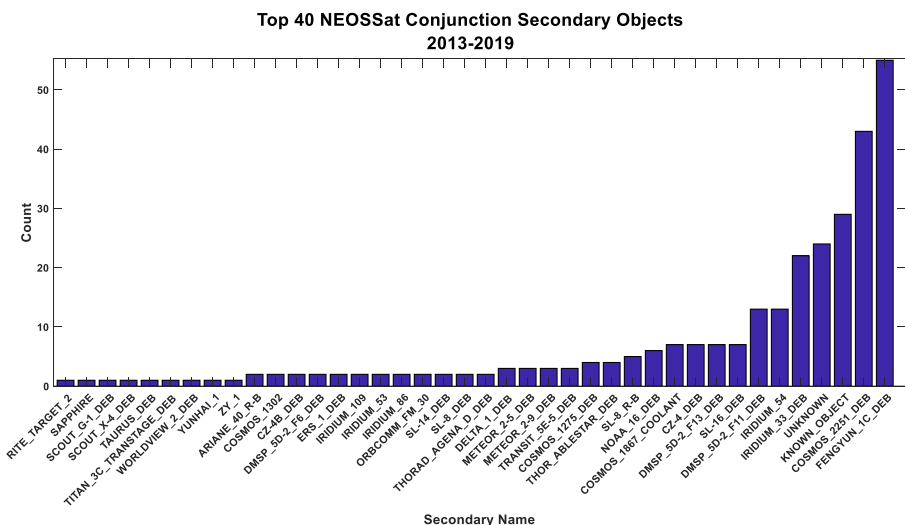

Fig. 1 Top 40 objects conjuncting frequently with NEOSSat

since its launch in 2013. Debris objects from FengYun 1C, Cosmos 2251, and Iridium 33 dominate the conjunction warnings issued to NEOSSat's satellite operations team. Objects positively identified as *debris* constitute ~60% of NEOSSat's conjunction history while another 7% are unknown objects not found in the public orbital catalog.

Since launch, the NEOSSat satellite operations team received 3710 conjunction warning messages from the 18th SPCS. From this, 345 unique conjunction events were identified, and the remaining messages were repeated, restated, or refined warnings of the same unique conjunction event prior to their TCAs. For each of these 345 unique conjunction events, the last warning message prior to TCA was used to characterize NEOSSat's conjunctions assuming it contains the most recent information on the conjunction.

In Fig. 2a, the occurrence of calculated NEOSSat PoC's greater than 10^{-10} are shown. Approximately 81% of these conjunctions had PoCs less than 10^{-6}, the warning threshold used by the Canadian Space Agency in their automated collision assessment processing. In Canada, satellite maneuvers are considered at PoCs exceeding 10^{-4}. NEOSSat's conjunction history has 9 events exceeding this limit, however NEOSSat is unequipped with a propulsion system for debris avoidance. The conjunction with the highest calculated risk to NEOSSat had a PoC of ~2.4×10^{-4}.
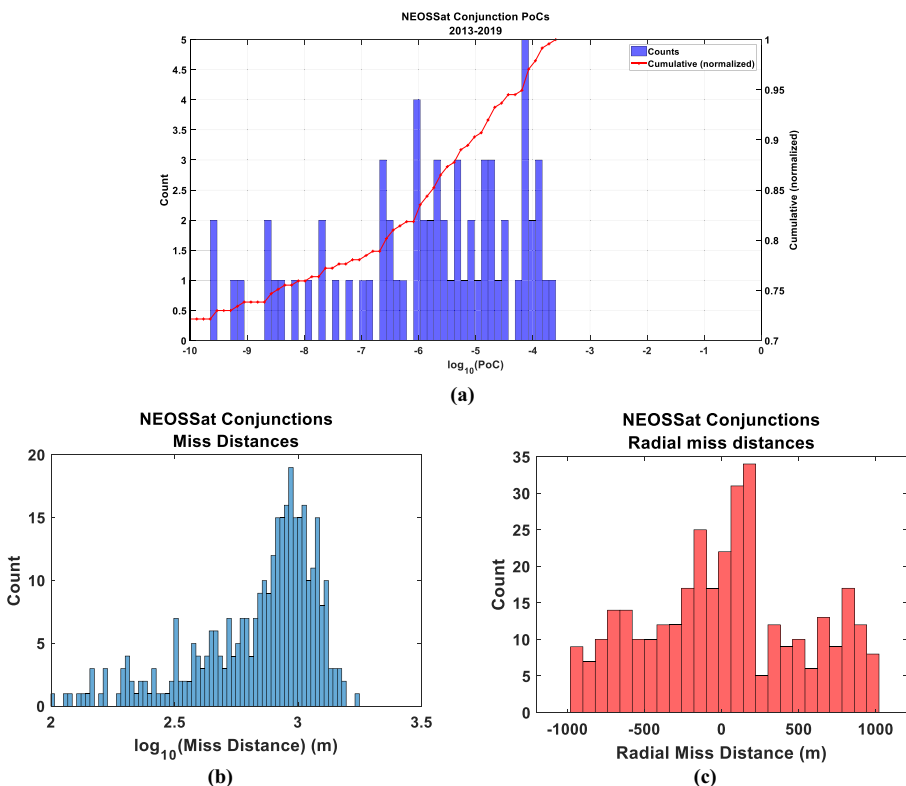

Fig. 2 (**a**) NEOSSat conjunction probabilities of collision. (**b**) Secondary object miss distances with NEOSSat, (**c**) Radial miss distance histogram showing the tendency of secondaries to pass below the vehicle

Considering all 345 unique close-approach events, a characterization of the conjunction geometry can be identified. NEOSSat and the secondary object conjuncting with it tend to have overall miss distances of ~1000 m (Fig. 2b) and is due to the 18 SPCS' conjunction screening algorithm examining a relatively large volume of 1x1x1 km³ around NEOSSat. A smaller portion of the conjunctions have miss distances of 100–400 m. The radial miss distances of NEOSSat conjunctions (Fig. 2c) show some interesting features. Conjuncting space objects tend to pass NEOSSat in three approximate altitude bands of approximately -750 m, 100 m and + 750 m with a general tendency to pass below the vehicle. This is attributed to the main secondary object sources of Feng Yun 1C debris, Cosmos 2251 debris, Known, Unknown and Iridium 33 debris objects.

NEOSSat conjunction warnings issued by 18 SPCS have a lopsided distribution of warning time, primarily driven by CSA's transition to the 18 SPCS Advanced Screening service for conjunction assessment in 2016 [2]. From 2013 to 2016, 18 SPCS provided NEOSSat conjunction warnings up to 3 days prior to TCA. Since CSA became a part of the Advanced Screening service, 18 SPCS now provides conjunction screening up to seven days prior to TCA and the resulting distribution of NEOSSat warning times is shown in Fig. 3. As of 2019, approximately 63% of all NEOSSat conjunctions have more than 6 days of warning time, offering the CSA satellite operations team more opportunities to perform analysis and trending of conjunction events. More recently, this generous warning time enables the NEOSSat mission science team to develop in-situ conjunction imaging experiments, as described in the next section.
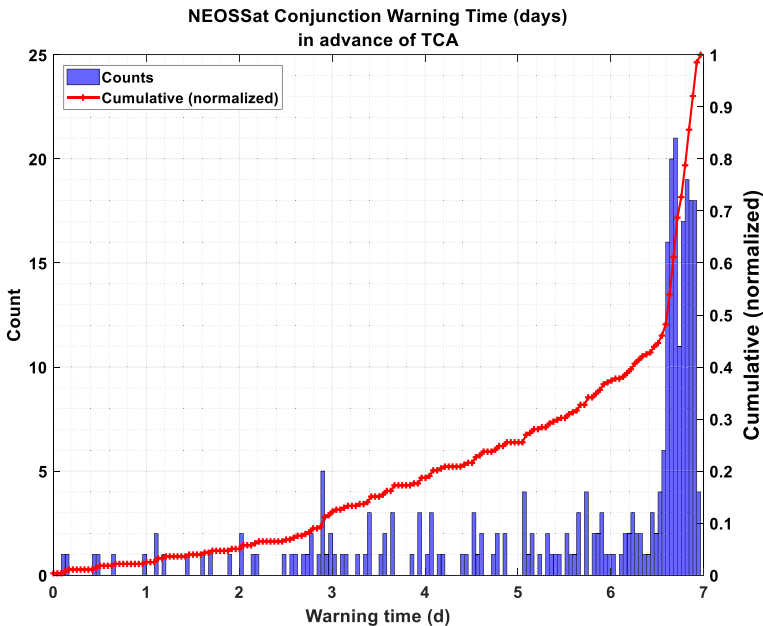

Fig. 3 NEOSSat conjunction warning times (days)

In-Situ Optical Characteristics of Leo Satellite Conjunctions

In 2018, NEOSSat began its first observations of objects forecasted to pass within a few kilometers of it in LEO. During a conjunction the secondary object appears in a near *constant-bearing, decreasing range* visibility condition in the few minutes prior to TCA. This causes the conjuncting secondary object to appear to have very small angular rates when observed at ranges from 4000 km down to 250 km. When a secondary passes within 250 km, NEOSSat is unable to track it as its angular rate accelerates drastically exceeding NEOSSat's attitude control capabilities. The time interval leading up to TCA creates short observing windows for NEOSSat to lock onto background star fields and acquire sidereal stare imagery on the advancing secondary object until it drifts off-frame during its pass. Figure 4 shows the approach geometry of the Spot-2 satellite and NEOSSat image of its approach during a conjunction in 2018.

There are two key photometric properties exhibited by conjuncting objects when tracked by a LEO observer:

Range Induced Brightening Conjuncting LEO objects exhibit strong, range-induced, brightening in the time leading up to TCA. Figure 5 shows the Spot-2 satellite during its illuminated approach toward NEOSSat. Bloom spikes are evident due to NEOSSat's CCD saturating on the very bright, approaching object. Careful selection of NEOSSat's CCD exposure time reduces the likelihood of saturation and is a strong consideration when planning observations on large conjuncting objects. Astrometry of saturated, blooming objects is possible, but less precision is expected in the resulting astrometric data.

Near-Constant Phase Angles The short ~4 min observing windows that NEOSSat can observe a LEO secondary object, either during the secondary's rapid approach or receding stage, constrains angular illumination geometry. A near-constant Sun/Object/Observer illumination phase angle geometry occurs and is atypical of optical space surveillance observations. The near rectilinear motion of the two objects, and the requirement to observe the secondary above the Earth's limb (>10 degrees elevation angle to avoid Earth's atmosphere) creates this quirk of conjunction observation
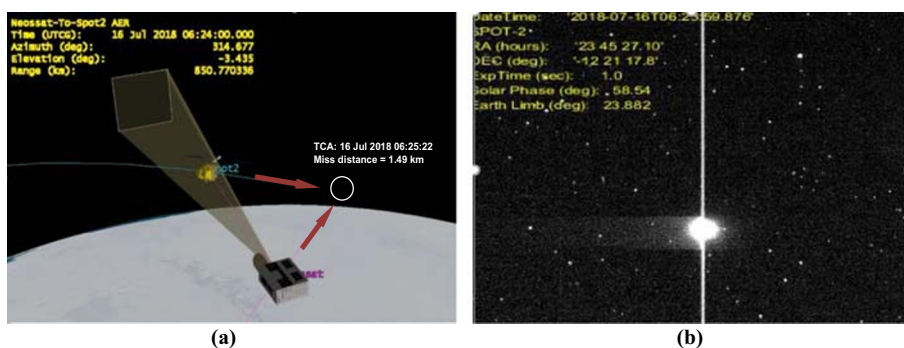

Fig. 4 (**a**): NEOSSat conjunction geometry with Spot-2. (**b**): Single frame of Spot-2 as observed by NEOSSat

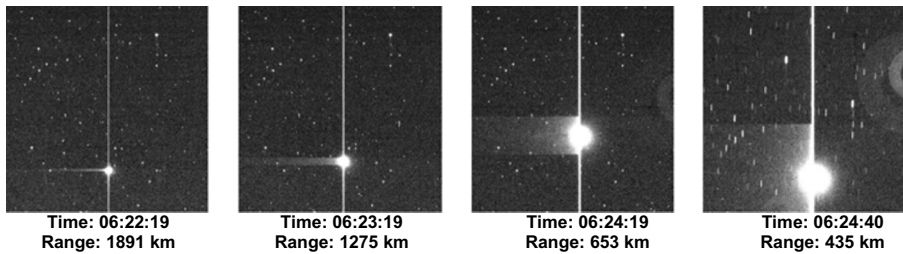| Time: 06:22:19 | Time: 06:23:19 | Time: 06:24:19 | Time: 06:24:40 |
| Range: 1891 km | Range: 1275 km | Range: 653 km | Range: 435 km |

Fig. 5 NEOSSat observations of the Spot-2 satellite conjunction on 16 July 2018

geometry. This enforces an operational constraint during NEOSSat conjunction observations as NEOSSat is designed to image outside of a 45° exclusion angle from the Sun. This forces the majority of NEOSSat's conjunction observations to be collected on objects during opposition or at phase angles less than 90°.

An observing campaign to characterize multiple space objects conjuncting with NEOSSat was performed. Close approaches forecasted by Celestrak's SOCRATES [5] conjunction forecasting web service were used to plan observations on objects making close passes to NEOSSat. Celestrak's use of a larger screening volume compared to 18 SPCS enabled frequent observing opportunities on secondary objects. This eases NEOSSat sensor planning as 18 SPCS' tighter screening volume (0.5 km radial for NEOSSat) reduces the frequency of observable events. This enables NEOSSat's separate exoplanet astronomy mission to be uninterrupted within NEOSSat's 36-h planning cycle. Table 1 summarizes the secondary objects observed by NEOSSat.

Figures 6a and 7a show the detected photometric characteristics of secondary objects observed by NEOSSat prior to conjunction. Figure 6b and Fig. 7b show the same detected magnitudes, but range normalized to 1000 km by subtracting $5log_{10}(R/R_0)$ where R is the detection range and R_0 is the normalization range. The figures are differentiated by *Payload* and *Debris* classes due to their inherent object size emphasizing their differing detected magnitudes (M_v). In both cases, objects were initially observed up to 4000 km from NEOSSat down to 250–500 km range. SARAL is a special case where it flew with NEOSSat for several orbital revolutions causing the densely packed appearance photometric data.[1] *Payloads* tend to span magnitude ranges of $M_v \sim 4.8$–11 and have relatively monotonically increasing light curves. An exception is Iridium 17 which appears to be rotating as glinting behavior is observed in its light curve. In Fig. 7, *Debris* objects span magnitude ranges of $M_v \sim 9$–16 and tend to have much higher variability likely due to their arbitrary shape and orientation during tracking.

Comparison of Fig. 6a and Fig. 7a highlights an operational consideration when observing small debris objects prior to TCA. *Debris* objects were detected by NEOSSat's image processing system only after they advanced approximately ~1000 km *closer* to NEOSSat compared to the much brighter *Payload* class of objects. This is understandable given that NEOSSat's image processing system's sensitivity is M_v 16. Debris objects must advance closer and brighten above NEOSSat's detection

---

[1] SARAL was not observed during closest approach but is included in Fig. 6 to illustrate the photometry of an object with a near zero approach angle appears with respect to a LEO observer.

Table 1 Close approach objects observed by NEOSSat

TCA (JDAY)	TCA (UTC)	Name	Secondary SSC#	Type	RCS Size	Approach Angle (deg)	Relative Velocity (km/s)	Miss distance (km)
2018–179	03:15:56	Orbcom B8	25416	PAYLOAD	Medium	100.6	11.49	2.99
2018–179	07:43:28	Iridium 17	24870	PAYLOAD	Large	47.6	6.02	4.874
2019–060	–	SARAL	39086	PAYLOAD	Large	–	–	–
2019–105	21:03:41	Cosmos 1275	13487	DEBRIS	Small	139.3	14.00	4.810
2019–107	18:22:18	FengYun1C	30109	DEBRIS	Small	142.9	14.21	6.236
2019–116	03:51:48	NOAA 8	13923	PAYLOAD	Large	138.2	13.91	4.81
2019–117	05:55:23	Transit 9	801	PAYLOAD	Large	81.08	9.7	56.24
2019–117	20:02:22	CZ-4 Deb	26294	DEBRIS	Medium	113.18	12.45	2.566
2019–118	08:56:24	Cosmos 1486	14240	PAYLOAD	Large	60.75	7.55	2.026
2019–118	01:44:01	CZ-4 Deb	20904	DEBRIS	Small	73.79	8.96	4.708
2019–123	20:56:56	Cosmos 1275 Deb	13026	DEBRIS	Small	135.80	13.85	1.957
2019–124	06:55:18	Cosmos 2251 Deb	34128	DEBRIS	Small	85.56	10.13	5.10
2019–125	14:00:11	Worldview-2 Deb	43368	DEBRIS	Small	92.85	10.82	23.46

Note: Four (4) additional debris objects were not detected by NEOSSat and are suspected to be fainter than NEOSSat's detection limit
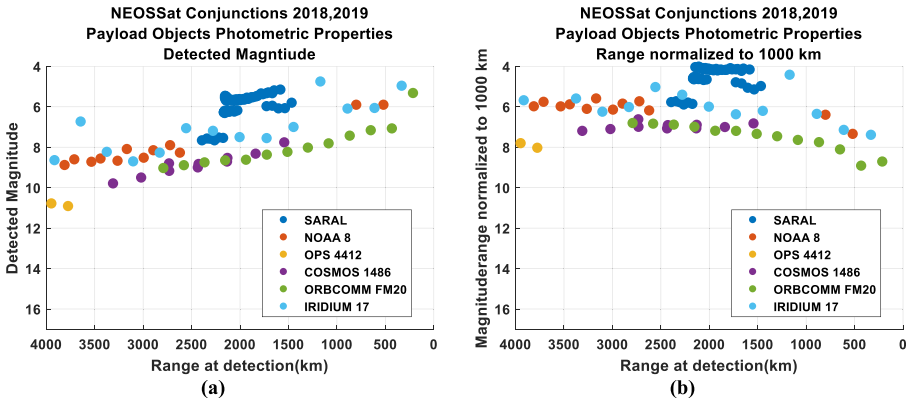
Fig. 6 (**a**): Photometric characteristics of conjuncting *Payload* objects observed by NEOSSat (**b**): Detected magnitudes range normalized to 1000 km

limit to be detected. Operationally, this lessens the amount of time to acquire data on debris objects, update orbits and make a maneuver decision if a satellite faces a high-risk conjunction scenario. During the observing campaign 4 additional debris objects were attempted but no detections were acquired. This suggests that these objects were either too faint to be detected by NEOSSat's instrument or had poor quality elsets in which to point NEOSSat's telescope.

The range normalized photometric plots Fig. 6b and Fig. 7b show several objects with relatively flat light curves suggesting that the range induced brightening effect is well-modelled by the inverse square range correction. Exceptions are visible in both *Payloads* and *Debris* classes such as Iridium 17, Orbcomm FM20 both Cosmos 1275 debris objects and CZ-4 debris. Their light curve variability suggests that during the short ~4 min observing windows, evidence of these objects reorienting (or tumbling) is detectable.

Given that debris avoidance in the final few minutes leading up to TCA is a challenging and likely impractical approach to collision mitigation, a better approach to secondary observation is described in the following section.
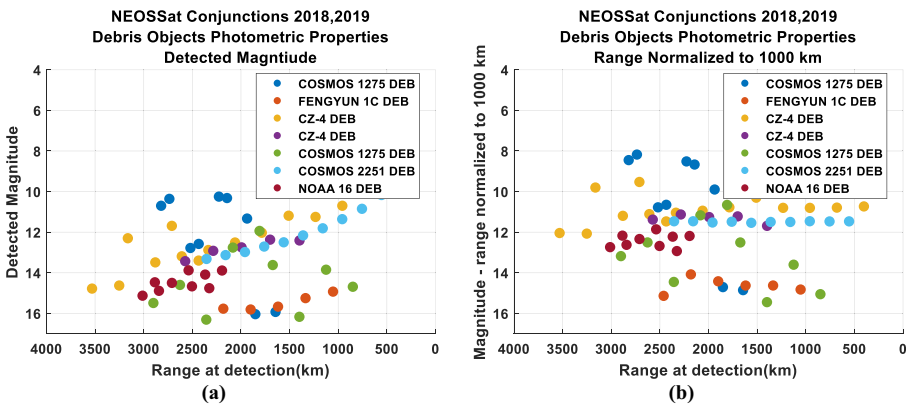

Fig. 7. (**a**): Photometric characteristics of close-approaching *Debris* objects observed by NEOSSat. (**b**): Detected magnitudes range normalized to 1000 km
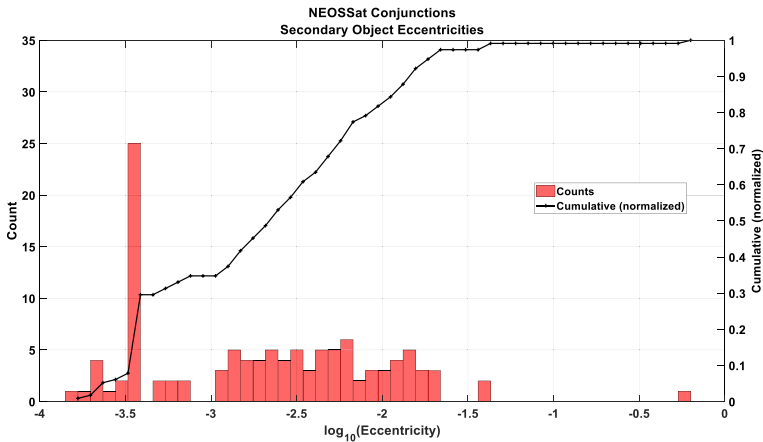
Fig. 8 Eccentricities of conjuncting objects where a CRAMs message was produced for NEOSSat. Most of the objects have eccentricities less than 0.01. The spike at log_{10}(eccentricity) ≈ -3.5 is due to cataloged, but "unknown" origin objects

A Half-Orbit Observing Strategy by Augmenting Pre-TCA Orbit State

Conjunctions tend to be envisaged as spontaneous, random events where two orbiting objects closely pass one another. Objects conjuncting with NEOSSat are mostly in circular orbits with 82% of the secondaries having eccentricities smaller than 0.01 (see Fig. 8) making the kinematics of conjunctions somewhat predictable and, fortuitously, increases the number of observing opportunities for NEOSSat to observe the secondary prior to TCA. Most conjuncting secondaries have a "*lead-up*" phase prior to conjunction with NEOSSat where the secondary makes multiple, diminishing range approaches at the *half-orbit* nodal intersections between the two objects prior to the closest pass at TCA. These opportunities are created due to the slight difference in orbital periods between NEOSSat and the secondary forming a synodic period of $T_{synodic} = T_1 T_2 / (T_1 - T_2)$ where T_1, T_2 are the orbital periods of the objects.

Two years of NEOSSat conjunction messages taken from the CSA's Conjunction Risk Assessment and Management System (CRAMS) [3] database was analyzed seeking conjunctions that could have been observed in by NEOSSat prior to TCA. CRAMS data includes TCA, the secondary object's Space Surveillance catalog number, range, errors and other metadata. Each conjunction was modelled in Satellite Tool Kit™ using an analysis period three days prior to TCA. NEOSSat's observing constraints [4] were then applied to determine intervals of visibility. A further constraint was enforced such that the secondary's phase angle was less than 90 degrees helping ensure the secondary was fully Sun-illuminated to increase the likelihood of detection of smaller objects.

Figure 9 shows NEOSSat's first observing opportunities on the secondary objects prior to TCA. The first opportunities tend to spike from 0.04 to 0.12 days indicating that ~96% of NEOSSat's conjunctions are visible with a lead time of ½ orbital revolution or more. 75% of the conjunctions had a lead time of more than 1 orbital revolution. Approximately 4% of the conjunctions had an observing lead time less than ½ orbital revolution and corresponded to the "Unknown" object population in LEO.
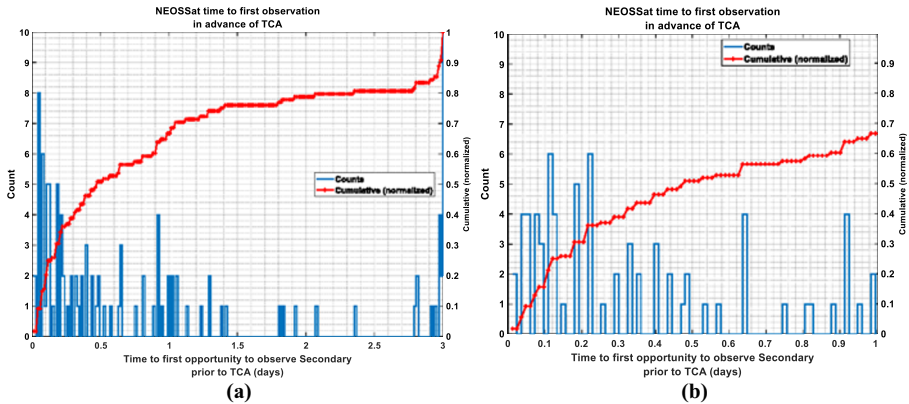
Fig. 9 (**a**): Observing opportunities on secondary objects from NEOSSat prior to TCA. (**b**): Same data showing the accesses from zero to one day of lead time

The *lead-up* phase generally offers multiple opportunities to observe the secondary in NEOSSat's near dawn-dusk sun synchronous orbit.

If NEOSSat was equipped with an image processor, orbit estimation and maneuvering capability, it is feasible that an autonomous debris observing strategy could be implemented as opportunities to observe the secondary exist prior to TCA. Such observations would differ from NEOSSat's typical rate-track mode geosynchronous observations.

Technique for Observing Conjuncting Space Objects Prior to TCA Space-based optical observations of conjuncting space objects are composed by pointing NEOSSat's imager into the relative velocity vector of the oncoming (or receding) object and ensuring the object is at least 10 degrees above the Earth's limb. This helps minimize detected light scattered from Earth's atmosphere when viewing near the illuminated portion of the Earth limb. This geometry creates a short-duration (< 4 min) sidereal-stare pointing condition for secondary objects 250–4000 km from NEOSSat. NEOSSat's imager then acquires imagery in rapid succession without needing to slew the telescope to follow the secondary. The imager is set to expose the CCD with exposures less than one second to reduce the likelihood of detector saturation when the secondary's apparent brightness increases by advancing toward the space-based observer.

If an on-orbit image processor were available onboard NEOSSat it would need to detect a brightening and slowly drifting object within the NEOSSat field of view. NEOSSat's astrometric accuracy in this mode is yet to be fully assessed, however, it is believed that the astrometric accuracy of this approach would be somewhat better than the 3.7″ performance achieved by NEOSSat on deep space objects using rate track mode (in 2×2 binning). This is due to the near elimination of rate-track angular rate mismatch that NEOSSat experiences [4] due to the slow frame rate of its imager. The slower angular acceleration of the target at longer ranges (>1000 km) would also lessen the target smearing effect on the target's centroid. To help reduce parallax error, the use of precision GPS ephemeris is required during such observations, especially on objects near the closest practical observing range limit of 250 km.

Half-Orbit Observing Strategy and Illustrative Orbit Estimation Findings

Recognizing that conjuncting objects are often visible to a space-based observer in the multiple half-orbits prior to TCA, NEOSSat conducted short observing campaigns on two conjuncting debris objects to test the observing approach and to characterize the behavior of the estimation process. As a full sensor astrometric calibration campaign is yet to be performed on satellites in LEO with NEOSSat, and some modelling mismatch exists due to the use of "estimated" debris uncertainties and estimation models - the following results are *illustrative*, rather than *definitive* in terms of the accuracy and performance of this technique during conjunction scenarios.

The first attempt was a debris object from a Japanese H-2A rocket (SSC# 43069, COSPAR: 2017-082E) with an orbit of apogee and perigee of 787×742 km. This object is listed as a small (< 0.1 m^2) radar cross section suggesting it has a characteristic length of ~0.3 m. NEOSSat made several close approaches with this object in the lead-up to its conjunction on 2 June 2019 20:02:54 and safely passed the object with a miss distance of 3.05 km. As this object's miss distance was well outside of the screening volume used by 18 SPCS, no CDM or CRAMs analysis was available. While this conjunction had a nearly zero-risk of collision, it offered an opportunity to test the half-orbit observing strategy prior to TCA on a bright debris object to collect astrometric observations for orbit estimation. Figure 10a shows the pass geometry at TCA while Fig. 10b shows the close approach nodes marked over Earth's North and South poles.

Four observing opportunities were available on the H2A debris prior to TCA and are shown in Fig. 11a. Photometric measurements collected by NEOSSat on the debris object are shown in Fig. 11b at intervals of 2 orbits, 1 orbit, and the half-orbit interval prior to TCA. The object was also observed during the terminal approach phase ($t = 0$ in Fig. 11). The brightness range of the debris object spans 10th to 12th magnitude suggesting that it is quite reflective. During the terminal pass, the object's brightness expands from 9th to 13th magnitude due to the longer window of observing opportunities available at that time. The absence of data at $t = 150$ *mins* is due to NEOSSat's attitude control
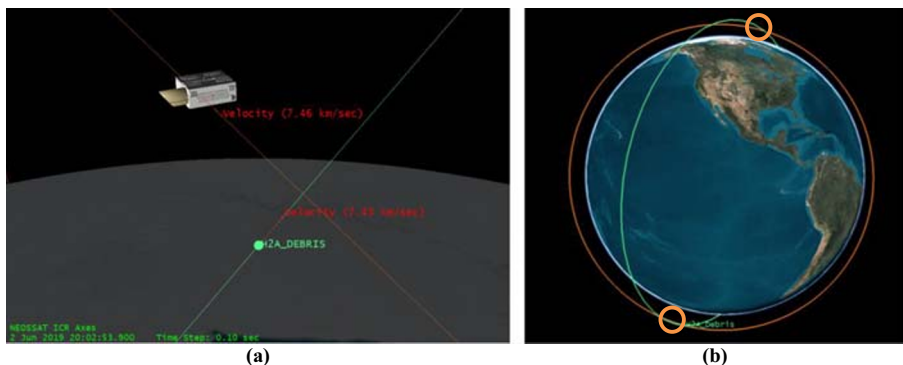

Fig. 10 (a): Pass geometry of the H2A debris object with NEOSSat. (b): Intersections of the debris object's orbit with NEOSSat's orbit over the North and South poles (marked)
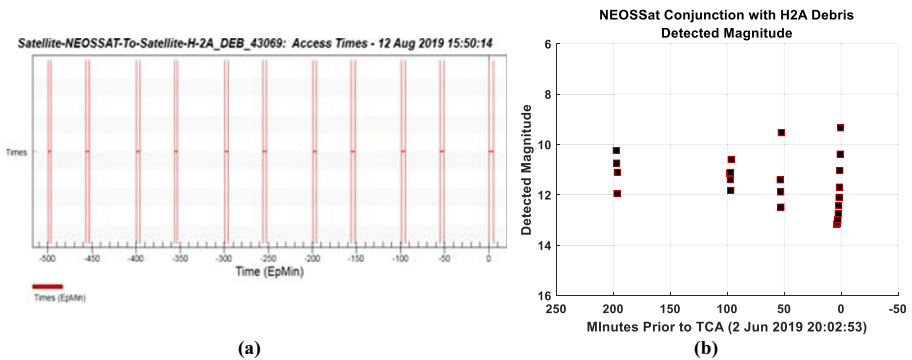
Fig. 11 (**a**) NEOSSat viewing opportunities on the H2A debris prior to TCA. (**b**): NEOSSat photometry of the H2A debris taken during the orbital opportunities 200 min prior to TCA. Note the reversed direction of the time axis where the conjunction occurs at $t = 0$

system running its momentum dumping process [6], hence no tracking data was collected. NEOSSat's momentum dumping process is not typical of most satellites in LEO therefore this observing interruption would not be an impediment for other satellites if they could observe the approaching secondary.

After measurements were downloaded ground-based orbit estimation on the H2A debris was performed. To illustrate NEOSSat self-estimating the orbit of the secondary using space-based optical measurements, a state was initialized for the H2A using two-line element set and covariance initialized consistent the typical position uncertainties of debris objects assessed by the CSA's CRAMS system. The H2A debris' initial position covariance was set to $P_{Debris} = \text{diag}(35^2, 1000^2, 10^2)$ m^2 and NEOSSat's to $P_{NEOSSat} = \text{diag}(10^2, 65^2, 10^2)$. Ground processing of tracking data used NEOSSat's right ascension and declination measurements to update the state and covariance using Orbit Determination Tool Kit's (ODTK) [7] extended Kalman filter. ODTK's force model was set to a 21×21 gravity field, object mass of 2 kg and 0.1 m^2 cross sectional area for drag force and solar radiation pressure modeling.

Figure 12 shows the change in the H2A debris' position uncertainty after all NEOSSat angles-only tracking data was added to the filter. Figure 13 shows the same covariance data on a logarithmic scale emphasizing the changes of the H2A's position uncertainty in all three flight axes. Radial and in-track position uncertainties diminish significantly during NEOSSat's observations to the 10 and 30-m level respectively. However, the H2A debris' cross-track uncertainty appears unaffected by NEOSSat's measurements. This appears to be due to the projected geometry of NEOSSat's imaging plane with respect to the flight axes of the secondary.

Figure 14 shows the covariance during the terminal phase of the H2A debris' closest approach with NEOSSat. The in-track and cross-track uncertainties show continually improving positioning knowledge when NEOSSat data was added to the filter prior to TCA. At 20:02:23 the in-track and radial position uncertainties are 25 m and 9 m respectively. The cross-track uncertainty remains unchanged even during the terminal phase of the conjunction.
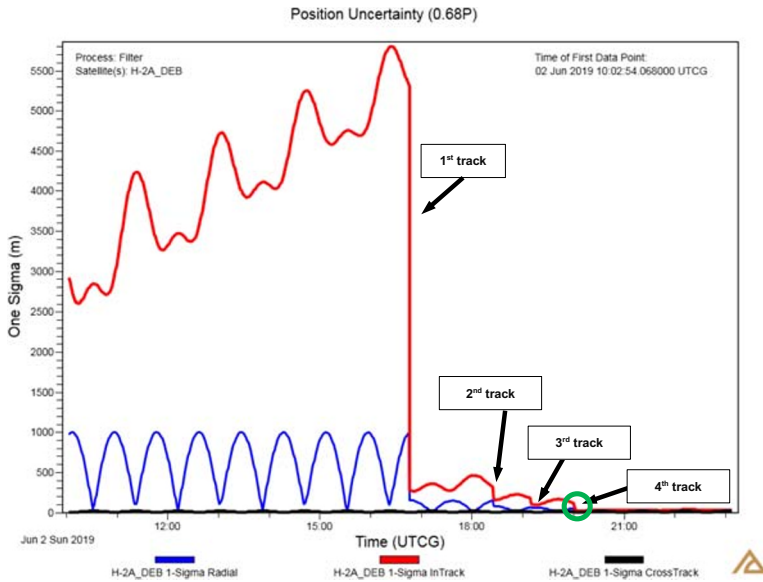
Fig. 12 H2A debris position uncertainty with NEOSSat tracking data used to improve positional knowledge. TCA is marked with green circle. Radial, in-track and cross-track position uncertainty is marked with blue, red, and black lines respectively

This example is illustrative of how the secondary's position uncertainty can be reduced prior to TCA using optical measurements. However, these results should not be interpreted as definitive in terms of the absolute performance achievable when the state and covariance is propagated to TCA using optical measurements on the secondary. This is due to the use of an initial state and covariance initialized from two-line elements sets and a 'characteristic' uncertainty typical of debris objects seen in Conjunction Data Messages.
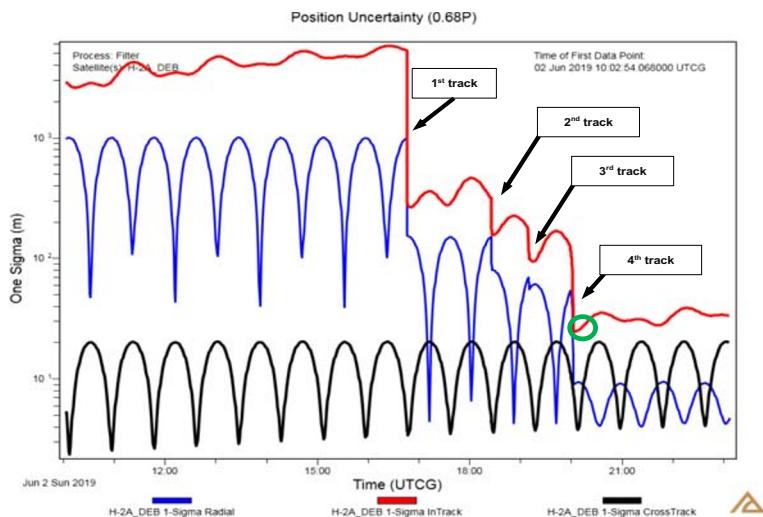
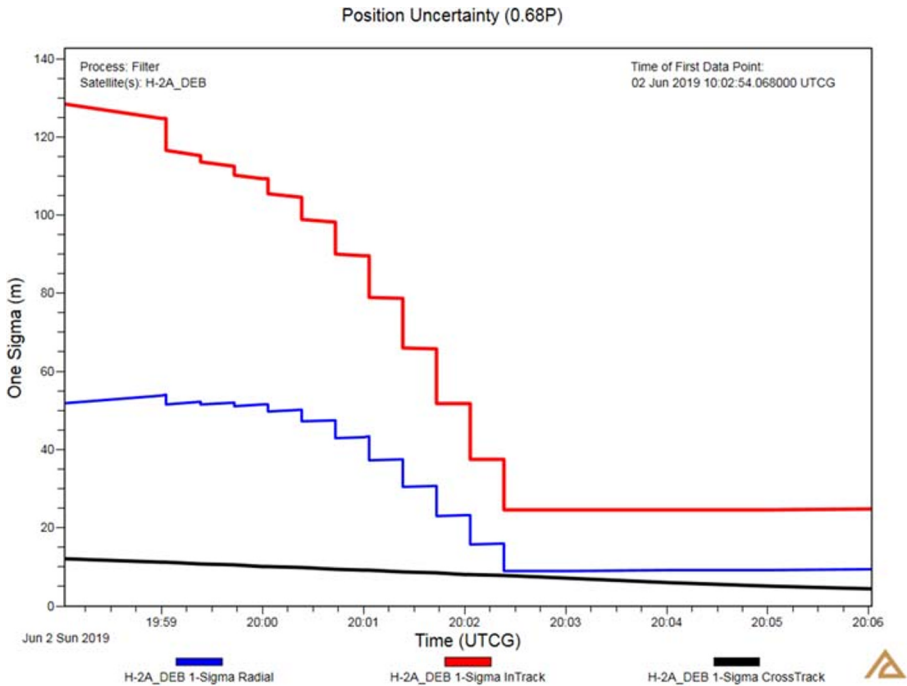**Fig. 13** H2A debris position uncertainty, logarithmic scale

Fig. 14 H2A position uncertainty during the terminal phase just prior to TCA at 20:02:54. Note that the cross-track uncertainty (black) is unaffected by the addition of space-based tracking data, whereas radial (blue) and in-track (red) position knowledge improves when measurement data is processed by the filter

Observations of an Object during a CRAMS-Based Warning

This case examines a more representative conjunction where a debris object was forecasted to approach NEOSSat within 18 SPCS' conjunction screening volume. A CDM was formed by 18 SPCS and the risk was evaluated by the CSA's satellite operations team. The conjunction of CZ-4 debris (SSC# 26294, COSPAR: 1999-057GG) was forecasted to occur on 27 Apr 2019 20:02:21.789 UTC with a miss
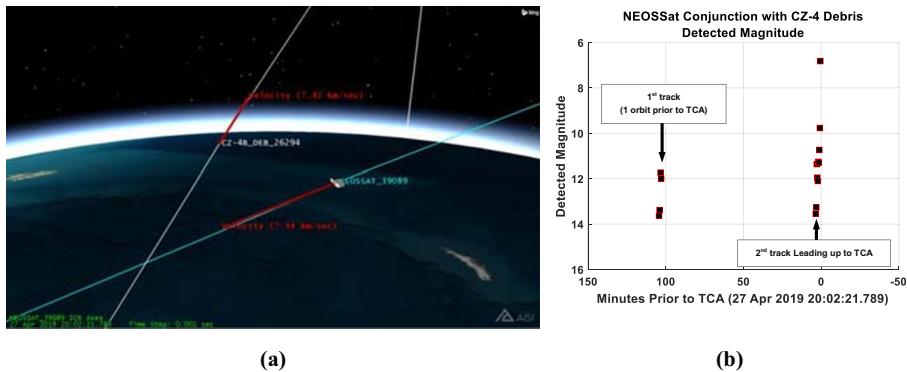

(a)

(b)

Fig. 15 (a) NEOSSat conjunction geometry with the CZ-4 debris. (b): NEOSSat photometry on the CZ-4 debris taken during 100 min and up to 4 min prior to TCA ($t = 0$)

distance of 1.08 km (see Fig. 15a). This object had an extremely low PoC given its relatively large miss distance, however the object was chosen for tracking. Photometric observations during the orbit prior to TCA (1st track) and during the terminal phase (2nd track) are shown. The object tends to be Mv 14 when it enters NEOSSat's detection capabilities and brightens by several magnitudes to M_v 7.

A state and covariance for the CZ-4 debris was provided by 18 SPCS three days prior to TCA. This state was used to initialize the orbit estimation process using the ODTK model described in the previous section. NEOSSat's space-based measurements were used to update the a-priori estimate. Figure 16 shows the object's position uncertainty, in a non-dimensionalized[2] scale relative to the radial position uncertainty. Improvement of the in-track (red) position knowledge again appears after processing NEOSSat's 4 measurements during the orbit prior to TCA and during the terminal phase. This time the radial position uncertainty, along with the cross-track position uncertainty shows no noticeable change when NEOSSat's measurements were added to the filter. NEOSSat's estimated angular measurement noise (~4 arcseconds), combined with the oblique observing geometry on the secondary object, appears to cause negligible reduction on the radial and cross-track position uncertainty in this case.

As in section 5, this estimation example is illustrative, rather than definitive of how optical measurements on the secondary object can improve position knowledge prior to TCA. This is due to modeling mismatch in the estimation process (filter versus least squares estimate for the CDM), the relative sparsity of observations, and that the angular astrometric accuracy of the NEOSSat sensor is yet to be fully established on LEO objects.

To mimic the case where a space-based sensor independently assesses the risk of conjunction by observing the secondary one full orbit prior to TCA, the filter was run with the 2nd track of observations ignored. The new state and covariance were propagated to TCA and a new PoC computed using Foster's probability of collision estimate [8]. Table 2 shows the change in the PoC after NEOSSat's observations updated the orbit. As this example had an exceptionally low initial risk of collision, one which an in-depth conjunction analysis is safely omitted, the addition and processing of NEOSSat's observations, finding a further 21 order-of-magnitude reduction in PoC is illustrative, but is not really indicative of a true level of risk reduction for the encounter. Table 2's results should not be considered definitive in terms of the level of actual performance until more test cases are processed. A more realistic test case would use a conjunction where the PoC exceeds the CSA's warning criteria of PoC $\sim 10^{-6}$ and NEOSSat observes the secondary to determine the true viability and utility of this approach. The CSA satellite operations team continues to monitor NEOSSat conjunctions for PoCs exceeding 10^{-6} to test this technique more fully.

Sensing Secondaries with Existing and New Satellites

NEOSSat was constructed with an optical payload specially designed to track other space objects. Many satellites are not equipped with this style of instrument; however, a commonly employed alternative exists. Star trackers, which perform attitude

---

[2] Covariance information is non-dimensionalized to preserve privacy of information provided by 18 SPCS.
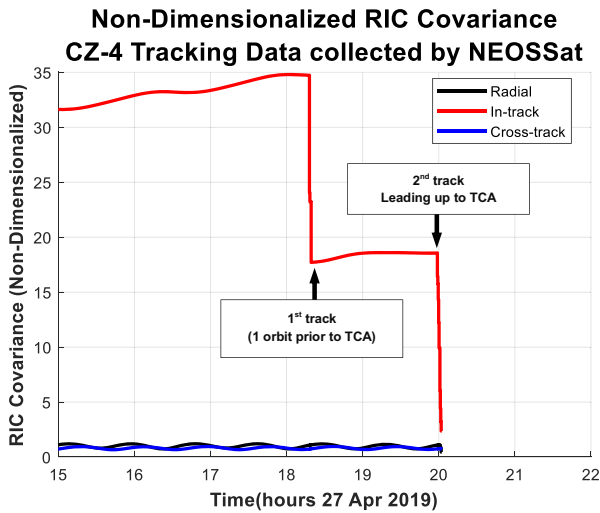
Fig. 16 CZ-4 position uncertainty after NEOSSat observations were processed by the filter. In-track positioning knowledge improves notably whereas radial and cross-track show no changes. Note the non-dimensionalized RIC scale is relative to the initial radial position uncertainty

measurement for many satellites, could theoretically be adapted for this type of observation. These specialized optical systems detect stars for high precision pitch/yaw and roll estimation, and some have imaging modes which could be adapted to detect, centroid and report conjuncting space objects. Some work examining star tracker utility for space surveillance has been performed [9, 10], but analysis of their application for use within conjunction derisk applications has not been considered.

Star trackers generally have small optical apertures (~2–10 cm), use short exposures (~ 0.1 s), have relatively large pixel pitches due to their large fields of view (~5°–20°), quantum efficiencies less than 60%, and tend to have higher read noise and dark currents compared to space surveillance instruments. Assuming a remote sensing satellite can point its usually zenith pointing star tracker(s) into the direction of an oncoming space object – an estimate of the detectability of a space object assuming a modest 2 cm aperture or more elaborate 10 cm aperture is shown in Fig. 17. For both, a dark current of 20 e⁻/pixel/s and read noise of 21e⁻ is assumed. The best pixel limiting magnitude estimate is found by taking a threshold Signal to Noise (SNR) ratio of 6 based on signal detection modelling from reference [11] to estimate the detectability of a space object.

Table 2 Probability of Collision for CRAMS warnings due to NEOSSat-collected orbital data

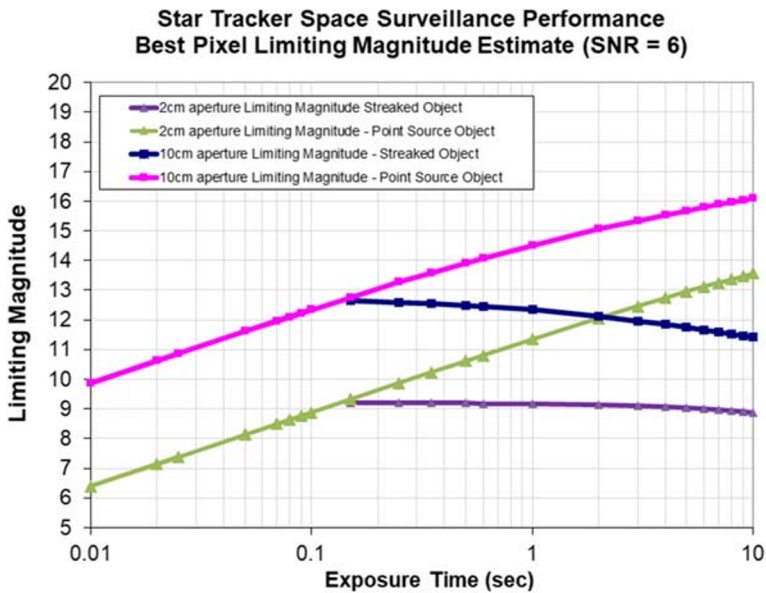|	Time to TCA (days)	$\log_{10}$(PoC)	Miss Distance (m)
1st Warning	6.8	−111	814
10th Warning	3.8	−120.07	1082
10th Warning + NEOSSat observations	3.8	−141.2	1110

Fig. 17 Star tracker space surveillance performance assuming 2 or 10 cm apertures, field of view of 20°, read noise of 21e⁻ and dark current of 20 e⁻/pixel/s and angular rate of 0.062°/s. Note that the streaked object limiting magnitudes split horizontally from the point source trend. This is due to the object's apparent angular rate streaking the object more than 1 pixel limiting detected photons per pixel during sidereal stare style imagery

A relatively modest 2 cm aperture star tracker could detect *payload*-class space objects to magnitude 8.8 during conjunctions using a 0.1 s exposure and still detect background stars to nearly the same magnitude. The photometric characteristics of *payloads* observed during conjunctions shown in Fig. 6a suggest they would be detectable by a small aperture star tracker. *Debris* objects are much fainter and likely undetectable unless a larger aperture of ~10 cm with a 2 s exposure is used achieving magnitude ~15. Star tracker pixels tend to be larger in comparison to dedicated space surveillance instruments which inherently senses more background sky noise – lessening their sensitivity to the space object being tracked. Star trackers may provide a means to perform optical measurements of conjuncting space objects prior to TCA, but careful consideration of their optical sensitivity, especially for debris objects, is required to make them viable for conjunction derisk on the thousands of debris objects known in Earth orbit.

Summary and Conclusion

Space-based optical measurements of orbiting objects conjuncting with a LEO observer were characterized by exploiting the near constant bearing, decreasing range observing geometry possible from a space-based platform. As NEOSSat is unable to perform on-orbit orbit estimation of other space objects, tracking data was downloaded and processed using ground-based SSA image processing and orbit estimation tools to

determine viability of independent collision assessment using a CDM as a cue. It was found that a small Sun-synchronous space surveillance telescope can optically detect the rapid advance of space objects prior to TCA if the secondary is Sun-illuminated and is elevated above Earth's limb such that astrometry can be performed on the space surveillance imagery. Both payload and debris objects were characterized in LEO with detections initially occurring at 4000 km range and rapidly approaching to 250 km range with apparent magnitudes spanning $M_v \sim 4.8$–11 for payloads and $M_v \sim 9$–16 for debris within a 4-min timescale. Four debris objects were undetected during this campaign and are suspected to be too small (faint) for detection by the NEOSSat instrument or not in field due to orbit uncertainty. Rapid range-induced brightening was observed for all conjuncting objects with several objects showing evidence of some rotational behavior. Payloads (large) conjuncting objects were regularly detectable up to 4000 km from NEOSSat. However, to detect smaller debris objects they needed to advance toward NEOSSat by an additional 1000 km to brighten enough to be detectable by NEOSSat's image processing system. To de-risk future conjunctions using optical measurements, this finding reinforces the need for sensitivity as debris objects represent most space objects in LEO.

A short investigation of the viability of orbit updates using space-based angles only tracking data was also performed. Since most space objects conjuncting with NEOSSat have near circular orbits, multiple repeat opportunities to observe the secondary prior to TCA is possible. An observing strategy employing opposition observations during the ½ orbit approaches prior to TCA helps increase the likelihood of detection of smaller objects. Observation processing on two different conjuncting space objects prior to TCA show improvement in the in-track position knowledge and partial improvement in the radial direction. Cross-track positioning knowledge showed little to no improvement in both tested conjunction cases. This is believed to be due to NEOSSat's measurement uncertainty and the oblique pass geometry of the secondary during its observation. A test case where the secondary was observed a full orbit prior to conjunction showed a reduction in the PoC, however these results should only be considered as illustrative of how this technique can be used for conjunction assessment. This is due to the initially miniscule initial risk of collision and the measurement uncertainty being much smaller than the separation between the two objects. A more realistic test case with PoCs of 10^{-6} or less is recommended to fully test this approach.

Finally, a short assessment of the viability of star trackers as sensors to perform conjunction observations was explored. Small aperture star trackers appear to be able to detect larger *payload* class objects during conjunctions. However, their viability for detecting debris objects during conjunctions is more limited unless the star tracker has a larger aperture, raising its sensitivity to fainter debris objects. It appears that satellites equipped with optical space surveillance cameras *could* help themselves in an increasingly risky orbital debris environment. With care taken toward debris object sensitivity and measurement precision, technical promise is growing for an optical alternative for secondary object orbit measurement during conjunctions in LEO.

Compliance with Ethical Standards

Conflict of Interest   The authors declare no conflict of, nor competing interest in the creation of this work.

References

1. 18th Space Control Squadron,: Spaceflight Safety Handbook for Satellite Operators Version 1.4. Joint Functional Space Component Command, Vandenberg, Air Force Base, https://www.space-track.org. Accessed 4 February 2019
2. Abbasi, V., Babiker, F., Doyon, M., Golla, D.: Close Encounters of an Advanced Kind: Lessons Learned and New Approaches in Collision Risk Assessment and Mitigation. 7th European Conference on Space Debris (2019). https://conference.sdo.esoc.esa.int/proceedings/sdc7/paper/1006/SDC7-paper1006.pdf
3. Babiker, F., Doyon, M., Abbasi, V.: Canadian Space Agency (CSA) collision risk assessment and mitigation system (CRAMS): sharing the development and operational challenges. SpaceOps Conference. **2012**, (2012). https://doi.org/10.2514/6.2012-1297827
4. Scott, R.L., Thorsteinson, S.E.: Key Finding from the NEOSSat Space-Based SSA Mission. AMOS Conference 2018, Maui Economic Development Board, Maui, HI, (2018)
5. Kelso, T.S.: Socrates: Satellite Orbital Conjunction Reports Assessing Threatening Encounters in Space. https://www.celestrak.com/SOCRATES/. Accessed 5 Aug 2019
6. Abbasi, V., Jackson, N., Doyon, M., Wessels, R., Sekhavat, P., Cannata, M., Gillett, R., Eagleson, S.: NEOSSat recovery following magnetometer and torque rod failure. SpaceOps. **2018**, (2018). https://arc.aiaa.org/doi/pdf/10.2514/6.2018-2664
7. Wright, J.: Orbit determination tool kit theory and algorithms. Analytical Graphics. https://www.agi.com/resources/white-papers/orbit-determination-tool-kit-theory-and-algorithms. Accessed 1 Aug 2019
8. Foster, J.L.: The analytic basis for debris avoidance operations for the international Space Station. In Proceedings of the Third European Conference on Space Debris, 19–21 March (2001)
9. Ettouati, I, Mortari, D., Pollock, T., "Space Surveillance Using Star Trackers", AAS/AIAA Space Flight Mechanics Meeting, Paper AAS 06–231, January 22–26 (2006)
10. Clemens, S., "On Orbit Resident Space Object (RSO) Detection Using Commercial Grade Star Trackers", Masters Thesis, York University Department of Earth and Space Science, May (2019)
11. Hejduk, M., "Satellite Detectability Modelling for Optical Sensors", AMOS Conference 2004, Maui Economic Development Board, Maui, HI., (2004)